Nanoscale Ruthenium(III) Complexes with Bioactive Ligands: Structural, Colloidal, and Dual Antimicrobial–Cytotoxic Investigations

Olga Impert,*[a] Natalia Czerniecka,[a] Natalia Balińska,[a] Barbara Kubiak,[a] Anna Kozakiewicz-Piekarz,[a] Oleksandra Pryshchepa,[b] Paweł Pomastowski,[b] Michalina Ehlert,[b] Maciej Witwicki,[d] Yogeswara Rao Pateda,[a,e] Erik Rakovský,[e] Anna Katafias,[a] and Rudi van Eldik*[a,c]

[a]Faculty of Chemistry, Nicolaus Copernicus University in Toruń, Gagarina 7, 87-100 Toruń, Poland
[b]Centre for Modern Interdisciplinary Technologies, Nicolaus Copernicus University in Toruń, Wileńska 4, 87-100 Toruń, Poland
[c]Department of Chemistry and Pharmacy, University of Erlangen-Nuremberg, Egerlandstrasse 1, 91058 Erlangen, Germany
[d]Faculty of Chemistry, University of Wroclaw, Joliot-Curie 14, 50-383 Wroclaw, Poland
[e]Comenius University in Bratislava, Faculty of Natural Sciences, Department of Inorganic Chemistry, Ilkovičova 6, 845 15 Bratislava, Slovakia.

*corresponding authors: oimpert@umk.pl and rudi.vaneldik@umk.pl

Table S1. Solubility of $[Ru^{III}Cl_4(Nic)_2]^-[(CH_3)_2NH_2]^+DMF$, **1**, complex.

Solvent	Yes/No	Solvent	Yes/No
Water	Yes	Ethyl acetate	No
Acetone	Yes	Diethyl ether	No
Toluene	No	^{i}PrOH	Yes
EtOH	Yes	^{i}BuOH	Yes
Chloroform	No	Cyclohexane	No
Acetonitrile	Yes	MeOH	Yes

Based on the data presented in Table S3, an **EtOH/cyclohexane** mixture was used to obtain nanoparticles of the complex.

Table S2. Solubility of $[Ru^{III}Cl_2(3\text{-}HPA)_2]^-[3\text{-}HH_2PA]^+(EtOH)_2$, **2**, complex.

Solvent	Yes/No	Solvent	Yes/No
Water	Yes	Ethyl acetate	Yes
Acetone	Yes	Diethyl ether	No
Toluene	No	^{i}PrOH	Yes
EtOH	Yes	^{i}BuOH	Yes
Chloroform	Yes	Cyclohexane	No
Acetonitrile	Yes	MeOH	Yes
n-hexane	No		

Based on the data presented in Table S4, an **EtOH/n-hexane** mixture was used to obtain nanoparticles of the complex.

Table S3. Selected bond lengths [Å] and angles [°] for $[Ru^{III}Cl_4(Nic)_2]^-[(CH_3)_2NH_2]^+DMF$, **1**, and $[Ru^{III}Cl_2(3\text{-}HPA)_2]^-[3\text{-}HH_2PA]^+(EtOH)_2$, **2**.

Bond lengths [Å]			
1		**2**	
Ru1-O1	2.035(2)	Ru1-N6^i	2.0896(12)
Ru1-O11	2.048(2)	Ru1-N6	2.0896(12)
Ru1-N15	2.061(2)	Ru1-Cl1	2.3486(4)
Ru1-N5	2.070(2)	Ru1-Cl1^i	2.3486(4)
Ru1-Cl2	2.3254(7)	Ru1-Cl2	2.3542(3)
Ru1-Cl1	2.3382(7)	Ru1-Cl2^i	2.3542(3)
Angle [°]			
1		**2**	
O1-Ru1-O11	86.83(8)	N6^i-Ru1-N6	180.0
O1-Ru1-N15	91.85(9)	N6^i-Ru1-Cl1	91.20(4)
O11-Ru1-N15	80.95(9)	N6-Ru1-Cl1	88.80(4)
O1-Ru1-N5	80.94(9)	N6^i-Ru1-Cl^i	88.80(4)
O11-Ru1-N5	92.68(9)	N6-Ru1-Cl1^i	91.20(4)
N15-Ru1-N5	170.67(9)	Cl1-Ru1-Cl1^i	180.0
O1-Ru1-Cl2	92.09(6)	N6^i-Ru1-Cl2	88.38(4)
O11-Ru1-Cl2	177.07(6)	N6-Ru1-Cl2	91.63(4)
N15-Ru1-Cl2	96.37(7)	Cl1-Ru1-Cl2	89.370(12)
N5-Ru1-Cl2	89.84(7)	Cl1^i-Ru1-Cl2	90.631(4)
O1-Ru1-Cl1	173.02(6)	N6^i-Ru1-Cl2^i	91.63(4)
O11-Ru1-Cl1	86.95(6)	N6-Ru1-Cl2^i	88.37(4)
N15-Ru1-Cl1	90.32(7)	Cl1-Ru1-Cl2^i	90.629(13)
N5-Ru1-Cl1	96.18(7)	Cl1^i-Ru1-Cl2^i	89.370(12)
Cl2-Ru1-Cl1	94.27(3)	Cl2-Ru1-Cl2^i	180.0

Symmetry code: (i) -x+1, -y+1, -z+1.

Table S4. Intra- and intermolecular interactions in $[Ru^{III}Cl_4(Nic)_2]^-[(CH_3)_2NH_2]^+DMF$, **1**, and $[Ru^{III}Cl_2(3\text{-}HPA)_2]^-[3\text{-}HH_2PA]^+(EtOH)_2$, **2**.

D-H…A	**d(D-H)**	**d(H…A)**	**<DHA**	**d(D…A)**
		1		
O1-H1A…O10	0.84	1.70	172.3	2.5396(18)
C7-H7A…Cl1^{vii}	0.95	2.62	142.3	3.4260(17)
C8-H8A…O1^{vii}	0.95	2.64	128.0	3.313(2)
C11-H11A…O3	0.95	2.60	129.4	3.287(2)
C14-H14A…O1^{viii}	0.98	2.89	119.6	3.483(2)

N16-H16B…Cl1	0.91	2.51	129.6	3.1685(4)
N16-H16B…Cl2	0.91	2.56	147.4	3.3654(18)
N16-H16B…Cl1^{vi}	0.91	2.51	129.6	3.1685(4)
N16-H16A…Cl2^{vi}	0.91	2.56	147.4	3.3654(18)
C15-H15A…Cl1^{vi}	0.98	2.92	113.9	3.4359(19)
C15-H15C…Cl2^{ix}	0.98	2.98	143.1	3.814(2)
		2		
C6-H6A…Cl1	0.95	2.85	118.8	3.409(3)
C6-H6A…Cl1^{i}	0.95	2.66	140.2	3.445(3)
C8-H8A…Cl2^{ii}	0.95	2.81	137.8	3.569(3)
O10-H10A…O3	0.84	1.88	145.2	2.618(3)
C16-H16A…Cl2	0.95	2.80	120.1	3.382(3)
C18-H18A…Cl1^{iii}	0.95	2.81	132.6	3.527(3)
C20-H20A…O13	0.84	1.90	145.0	2.636(3)
C23-H23A…O36	0.84	1.61	177.0	2.451(3)
N25-H25A…O11	0.88	1.90	162.6	2.748(3)
C26-H26A…Cl1	0.95	2.89	143.6	3.694(3)
C27-H27A…Cl2^{i}	0.95	2.87	171.2	3.812(3)
C28-H28A…O20^{iv}	0.95	2.55	141.9	3.347(4)
O30-H30A…O13^{v}	0.84	2.34	122.8	2.887(3)
O30-H30A…O21	0.84	1.96	143.1	2.678(3)
C31-H31B…O1	0.98	2.56	151.3	3.449(5)
O33-H33A…O3	1.06	1.79	154.2	2.775(3)
O36-H36A…O33	0.91	1.70	165.5	2.591(3)

Symmetry code: (i) -x+1, -y+1, -z; (ii) -x, -y+1, -z; (iii) -x+1, -y, -z; (iv) x, y+1, z; (v) -x+1, -y+1, -z+1; (vi) -x+1, y, -z+1/2; (vii) x, y-1, z;

Table S5. Average crystallite sizes and elastic strain for $[Ru^{III}Cl_4(Nic)_2]^-[(CH_3)_2NH_2]^+DMF$ **(1)**$_{Str-30}$ and $[Ru^{III}Cl_2(3\text{-}HPA)_2]^-[3\text{-}HH_2PA]^+(EtOH)_2$ **(2)**$_{Str-15}$

Complex Nanoparticles	2θ [°]	FWHM [°]	Scherrer Equation		Williamson-Hall Plot		
			Crystallite size D [nm]	average D [nm]	average D [nm]	Lattice strain ε	average dislocation density (lines/m^2)×10^{12}
NPs(1) $_{Str-30}$	13.7416	0.5353	14.9482	18	15	−0.0010 (0.1%)	4.44
	21.2173	0.5353	15.0989				
	22.721	0.5353	15.1374				
	23.8224	0.2318	35.0263				
	25.3219	0.5353	15.2107				
	26.8159	0.5353	15.2567				
	29.0541	0.5353	15.3310				
NPs(2) $_{Str-15}$	11.1092	0.4508	17.7058	24.22	8.92	−0.0126 (1.3%)	12.57
	12.2535	0.5244	15.2363				
	12.7962	1.3529	5.9088				
	14.7812	0.2318	34.5593				
	17.8866	0.2209	36.4059				
	18.5263	0.2386	33.7354				
	19.159	0.2584	31.1789				
	24.0336	0.5353	15.1733				
	26.5775	0.2912	28.0318				

Table S6. Principal g tensor components calculated at the DFT theory level.

Complex	Functional	g_z	g_y	g_x
1	PBE0	2.02	2.32	2.43
	PBE0-50	1.99	2.47	2.50
	TPSSh	2.04	2.22	2.31
	TPSS0	2.02	2.27	2.33
	TPSSh-50	1.98	2.40	2.41
	BHANDHLYP	1.98	2.51	2.54
	Exp.	*1.34*	*2.56*	*2.69*
2	PBE0	1.99	2.29	2.35
	PBE0-50	1.95	2.37	2.42
	TPSSh	2.00	2.21	2.25
	TPSS0	1.99	2.24	2.28
	TPSSh-50	1.96	2.31	2.36
	BHANDHLYP	1.95	2.39	2.45
	Exp.	*1.67*	*2.45*	*2.57*

Comment to Table S6: As expected [1], deviations from experimental values are evident, which can be attributed to limitations in predicting electronic excitations and an overestimation of spin density transfer from the metal to the ligands [2,3]. As observed in our previous studies [1], the best agreement between theory and experiment was obtained using the BHandHLYP functional, which includes 50% exact Hartree-Fock exchange. Additionally, increasing the Hartree-Fock exchange to 50% in PBE0 and TPSS0 significantly improved the accuracy of the computed *g* values. A similar enhancement in DFT accuracy was previously reported for predicting hyperfine couplings in *5d* hexafluoridocomplexes of Re(IV) and Ir(IV) [4].

1. O. Impert, A. Kozakiewicz-Piekarz, A. Katafias, M. Witwicki, U. K. Komarnicka, K. Kurpiewska, R. van Eldik, Mixed-valence outer-sphere Ru^{II}/Ru^{III} ion-pair complexes. Synthesis, experimental, and theoretical studies, Polyhedron, 2022, **223**, 115939.
2. (34) S. Kumar, R. P. Sharma, P. Venugopalan, M. Witwicki, V. Ferretti, Synthesis, Characterization, Single Crystal X-Ray Structure, EPR and Theoretical Studies of a New Hybrid Inorganic-Organic Compound $[Cu(Hdien)_2(H_2O)_2](Pnb)_4 \cdot 4H_2O$ and Its Structural Comparison with Related $[Cu(En)_2(H_2O)_2](Pnb)_2$, J. Mol. Struct., 2016, **1123**, 124.
3. (35) F. Neese, Sum-over-States Based Multireferenceab Initio Calculation of EPR Spin Hamiltonian Parameters for Transition Metal Complexes. A Case Study, Magn. Reson. Chem., 2004, **42**, S187.
4. (36) P. A. B. Haase, M. Repisky, S. Komorovsky, J. Bendix, S. P. A. Sauer, Relativistic DFT Calculations of Hyperfine Coupling Constants in 5d Hexafluorido Complexes: $[ReF_6]^{2-}$ and $[IrF_6]^{2-}$, Chem. - Eur. J., 2018, **24**, 5124.

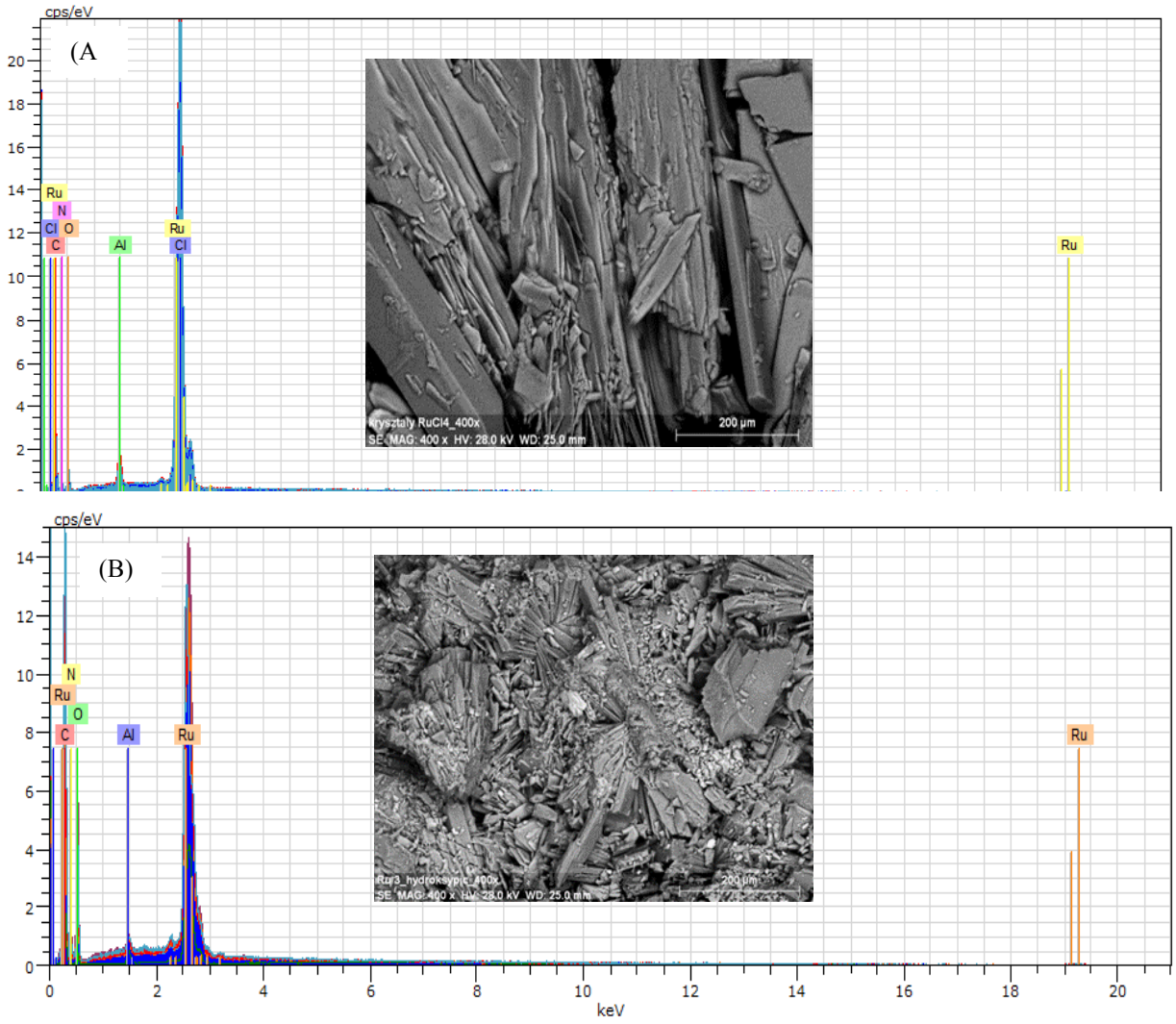

Figure S1. EDX patterns and SEM micrographs of the (A) $[Ru^{III}Cl_4(Nic)_2]^-[(CH_3)_2NH_2]^+DMF$, **1**, and (B) $[Ru^{III}Cl_2(3\text{-}HPA)_2]^-[3\text{-}HH_2PA]^+(EtOH)_2$, **2**.

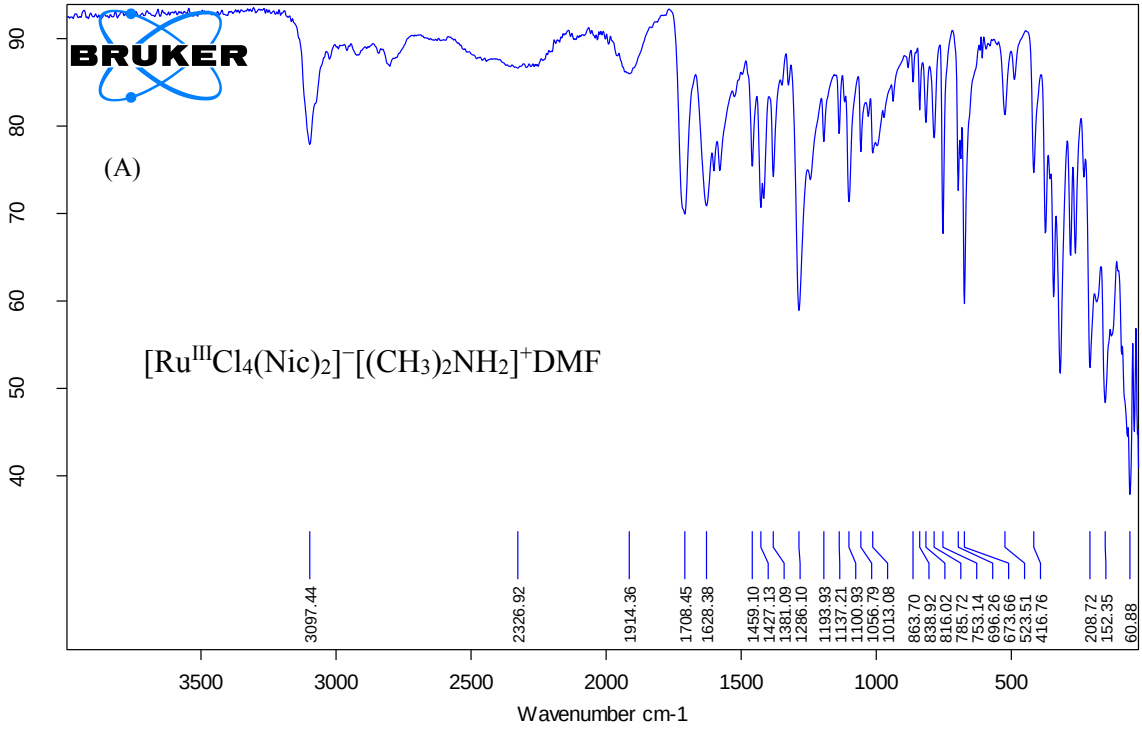

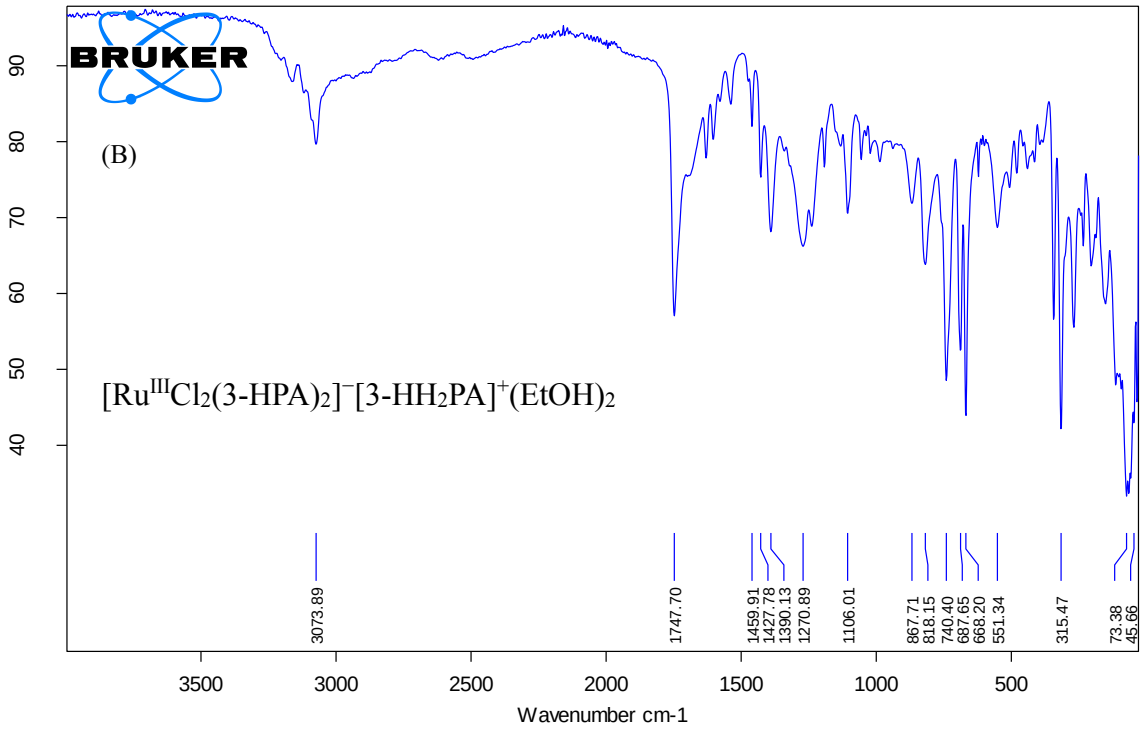

Figure S2. IR spectrum for (A) the $[Ru^{III}Cl_4(Nic)_2]^-[(CH_3)_2NH_2]^+DMF$ and (B) $[Ru^{III}Cl_2(3\text{-}HPA)_2]^-[3\text{-}HH_2PA]^+(EtOH)_2$ complexes.

92.28 n

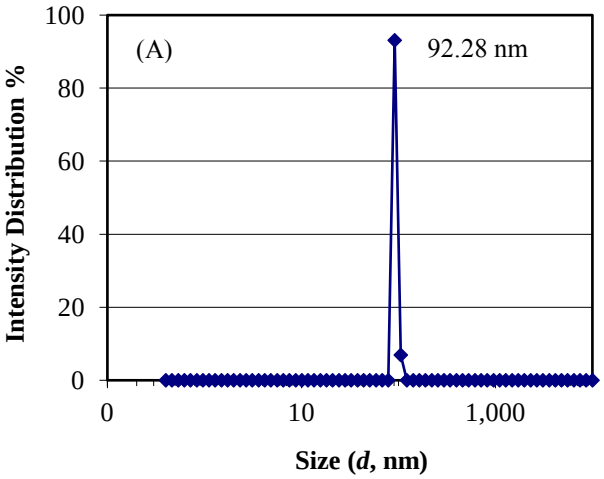
(A)
92.28 nm
Intensity Distribution %
Size (d, nm)

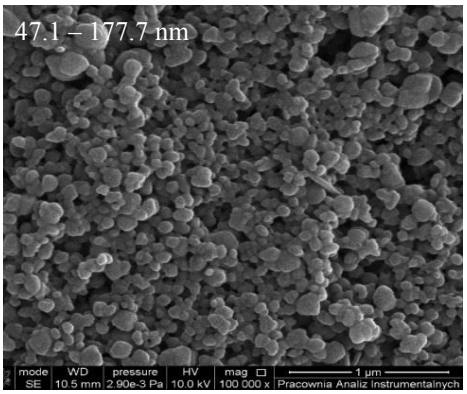
47.1 – 177.7 nm

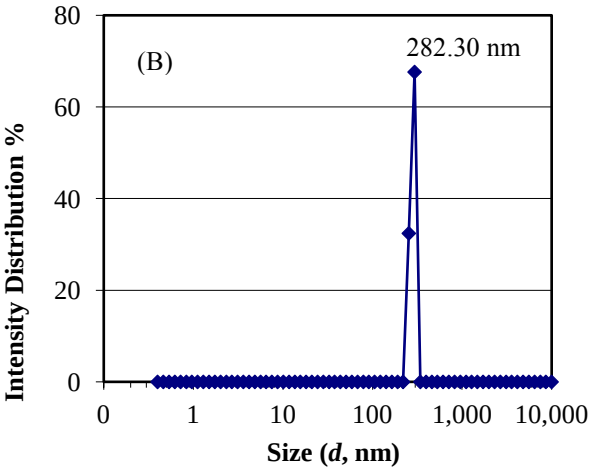
(B)
282.30 nm
Intensity Distribution %
Size (d, nm)

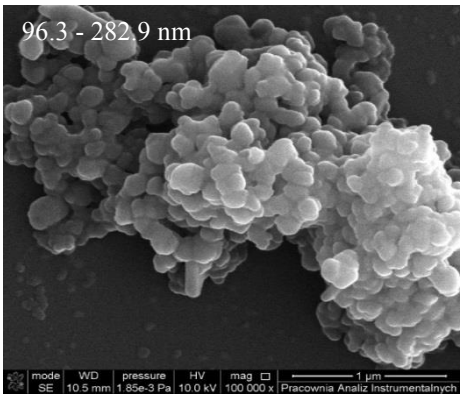
96.3 - 282.9 nm

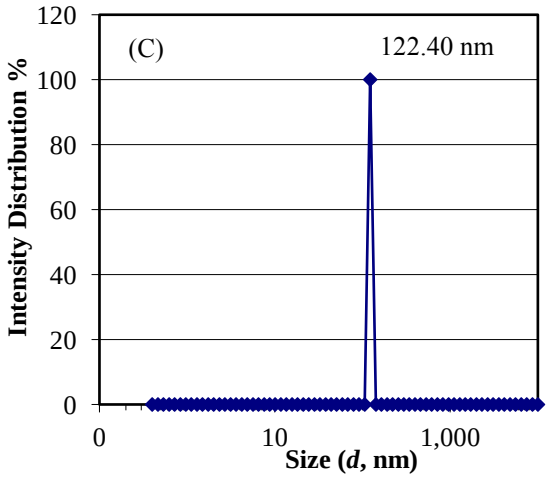
(C)
122.40 nm
Intensity Distribution %
Size (d, nm)

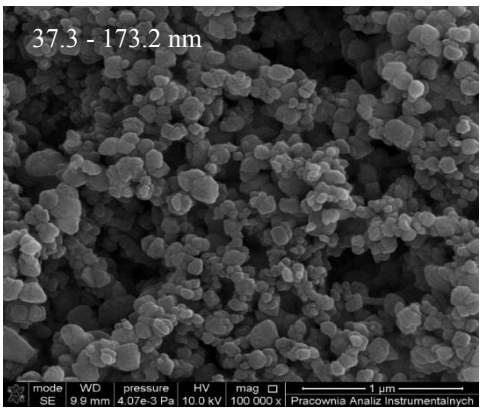
37.3 - 173.2 nm

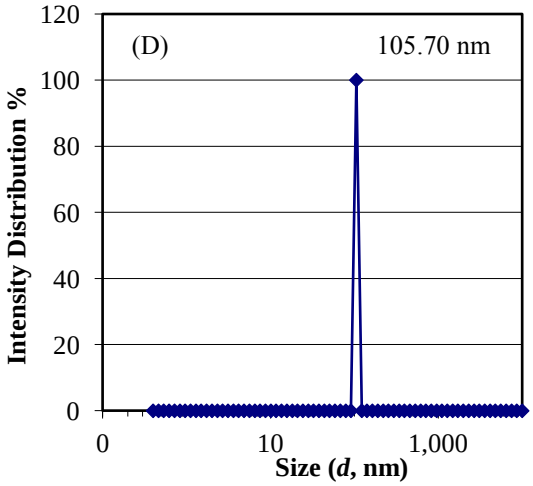
(D)
105.70 nm
Intensity Distribution %
Size (d, nm)

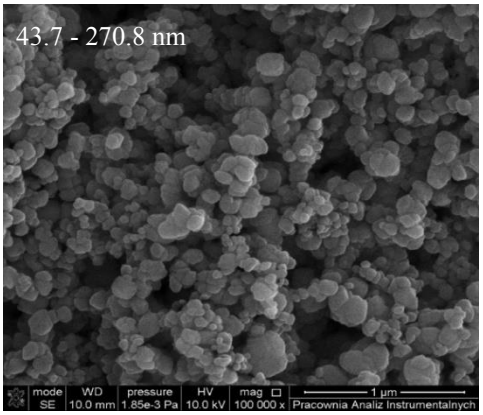
43.7 - 270.8 nm

Figure S3. Hydrodynamic size and SEM image of NPs of $[Ru^{III}Cl_4(Nic)_2]^-[(CH_3)_2NH_2]^+$DMF obtained from the anti-solvent method; stirring time A) 10, B) 15, C) 30 and D) 60 minutes.

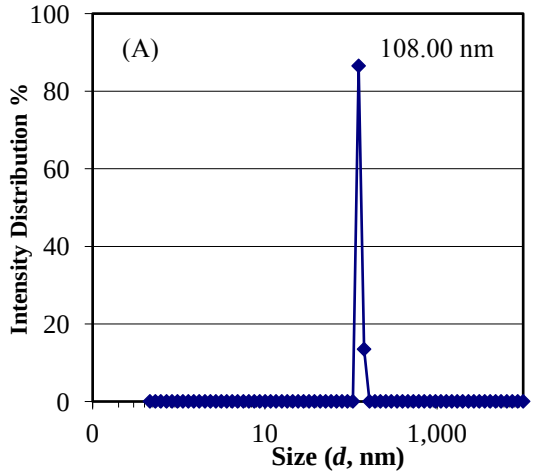

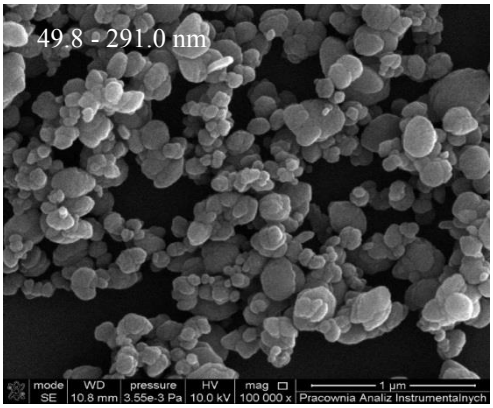

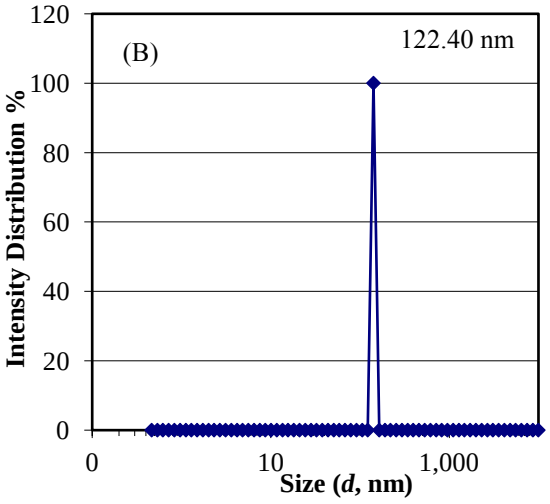

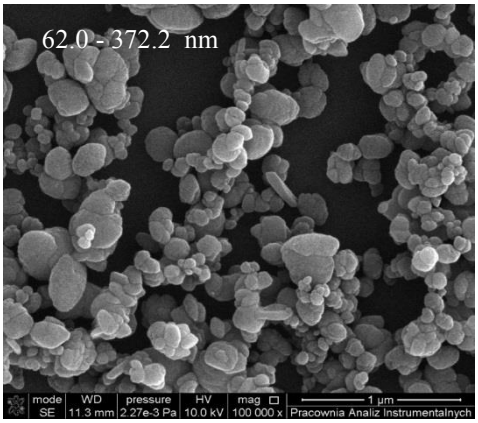

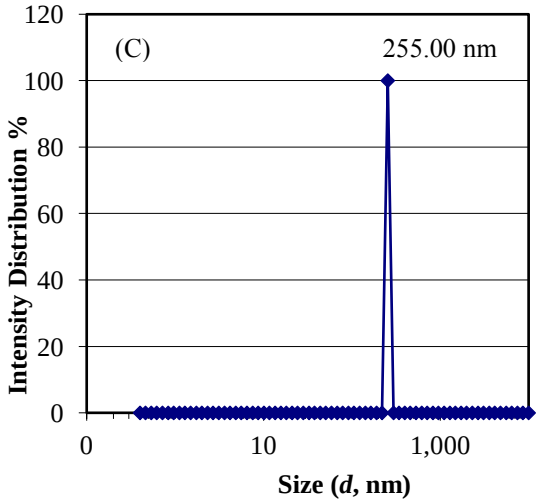

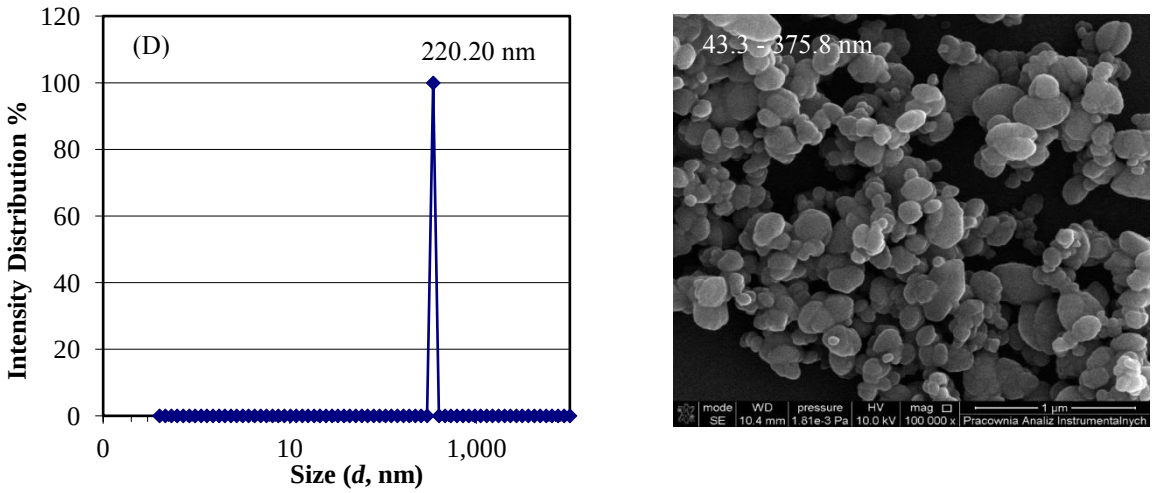

Figure S4. Hydrodynamic size and SEM image of NPs of $[Ru^{III}Cl_4(Nic)_2]^-[(CH_3)_2NH_2]^+$DMF obtained from the anti-solvent method; sonication time: (A) 10, (B) 15, (C) 30 and (D) 60 minutes.

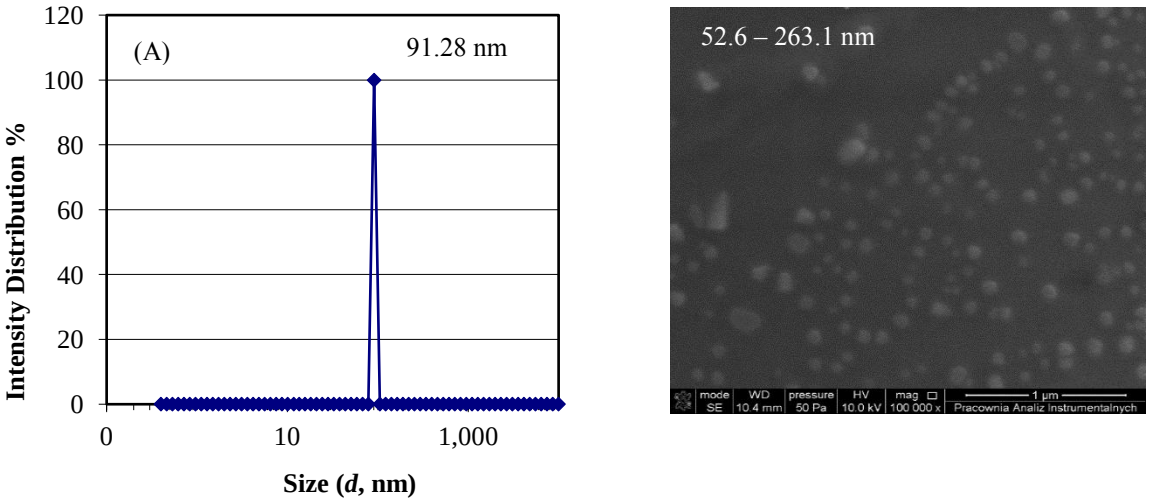

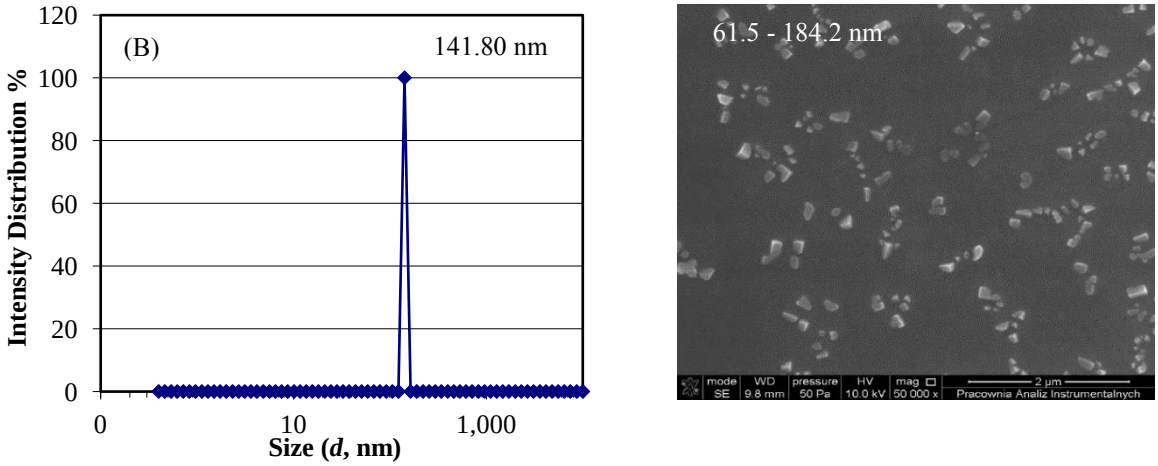

.

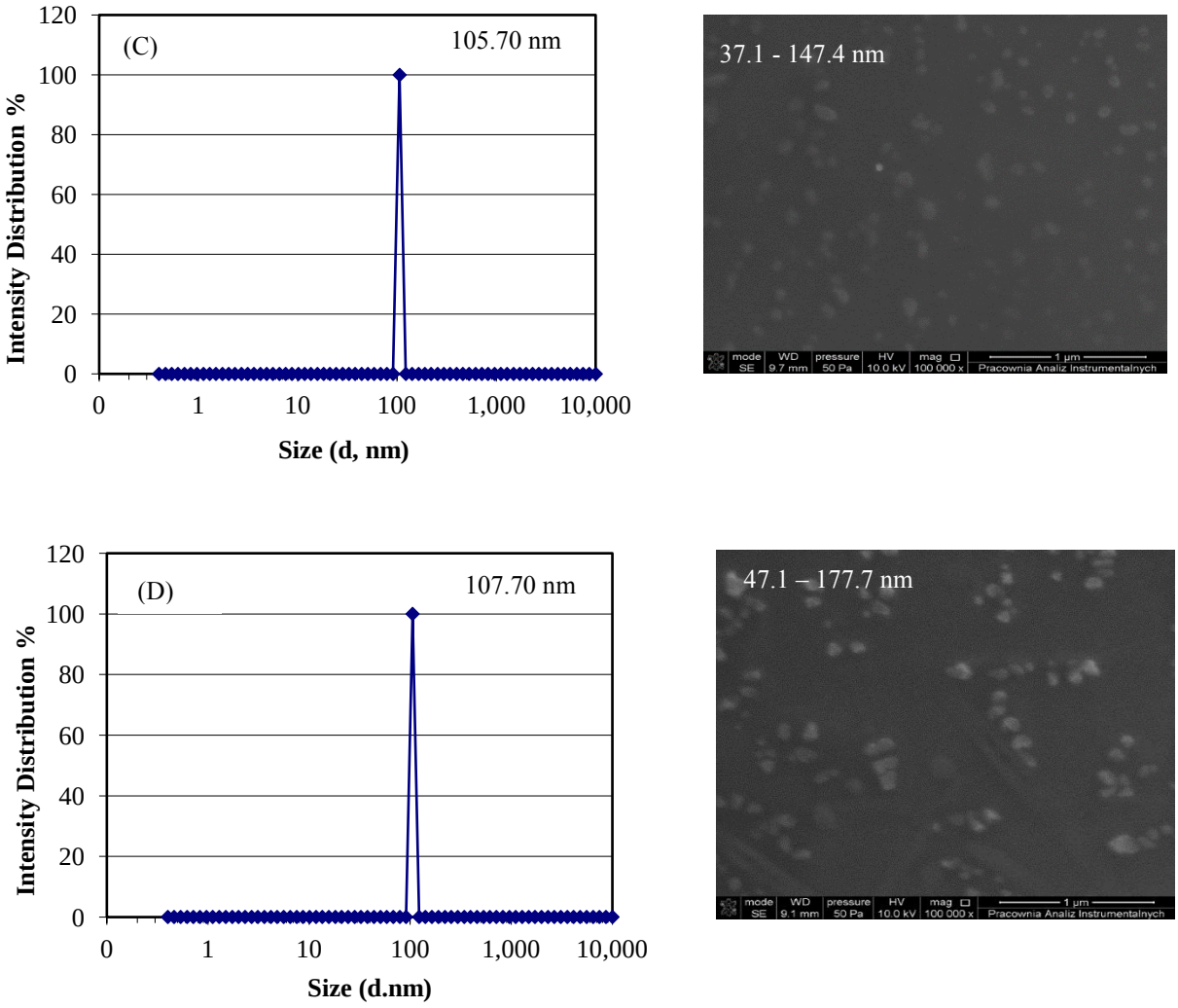

Figure S5. Hydrodynamic size and SEM image of NPs of $[Ru^{III}Cl_2(3\text{-}HPA)_2]^-[3\text{-}HH_2PA]^+(EtOH)_2$ obtained from the anti-solvent method; stirring time A) 10, B) 15, C) 30 and D) 60 minutes.

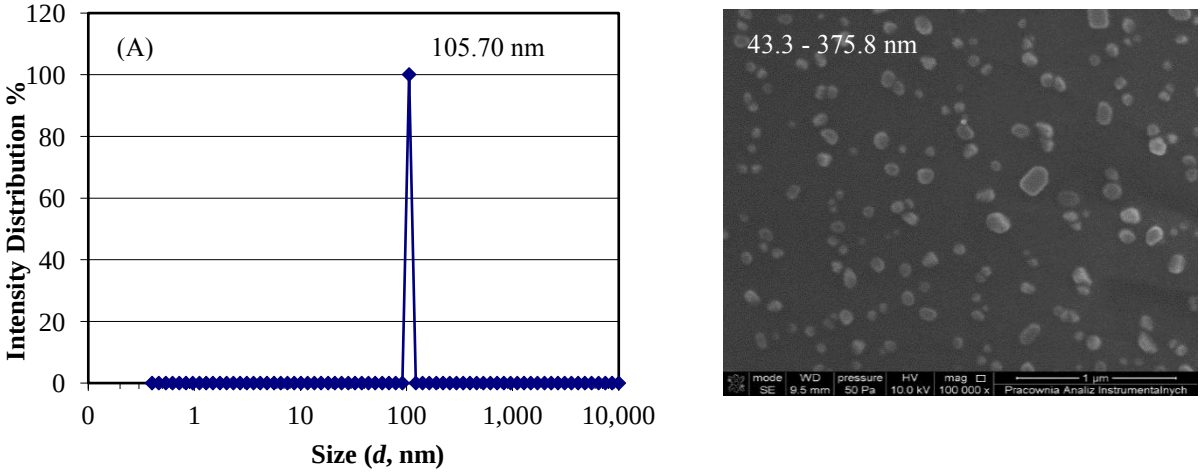

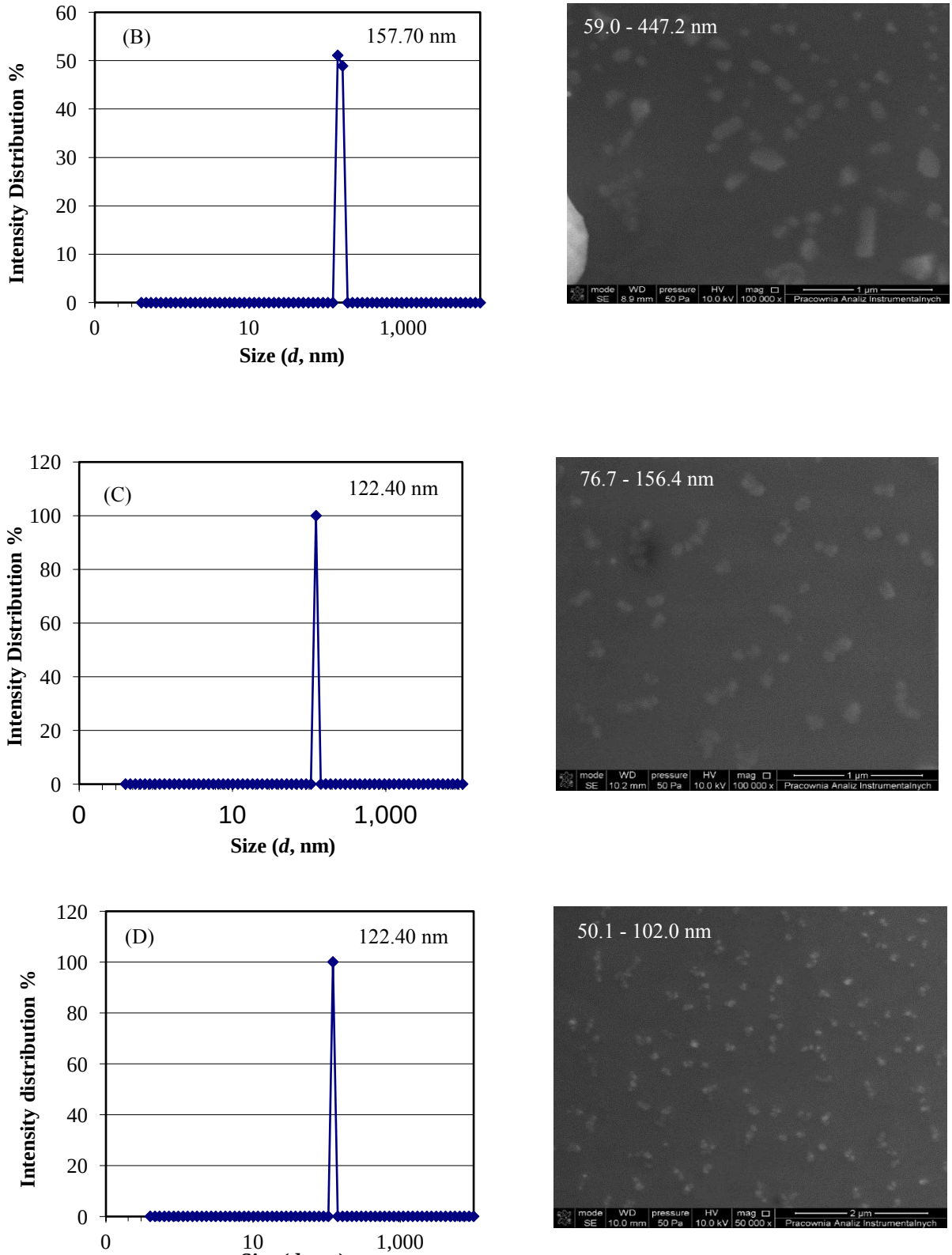

Figure S6. Hydrodynamic size and SEM image for NPs of $[Ru^{III}Cl_2(3\text{-}HPA)_2]^-[3\text{-}HH_2PA]^+(EtOH)_2$ obtained from the anti-solvent method; sonication time: (A) 10, (B) 15, (C) 30 and (D) 60 minutes.

(A)

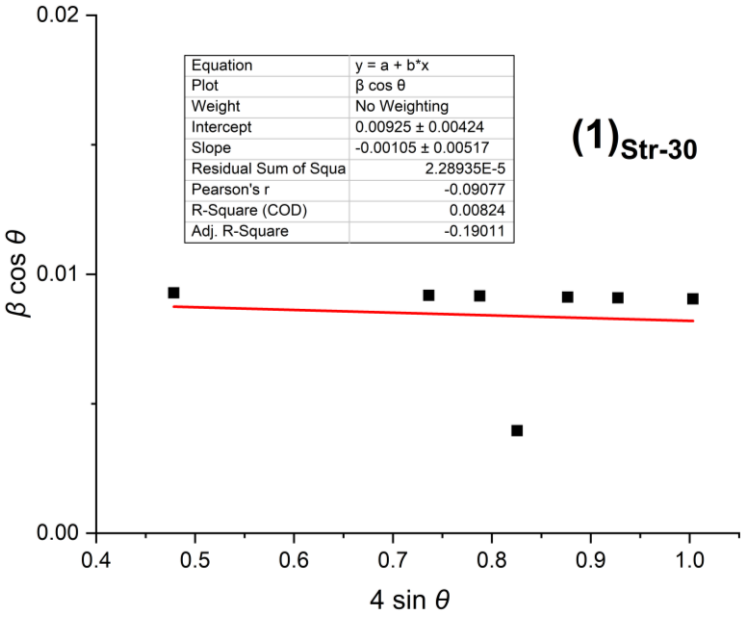

(B)

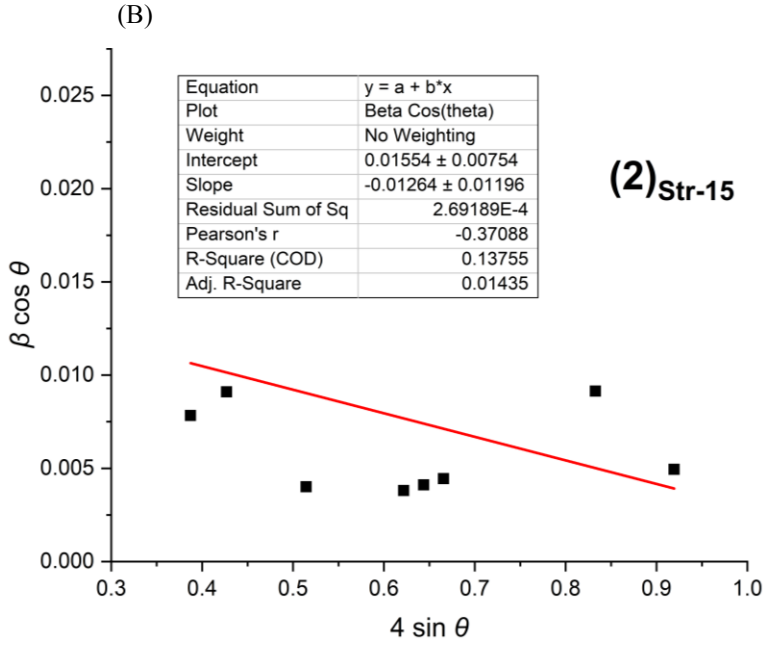

Figure S7. Williamson-Hall plots for NPs (A) $[Ru^{III}Cl_4(Nic)_2]^-$ $[(CH_3)_2NH_2]^+$DMF **(1)**$_{Str-30}$ and (B) $[Ru^{III}Cl_2(3\text{-}HPA)_2]^-[3\text{-}HH_2PA]^+(EtOH)_2$ **(2)**$_{Str-15}$

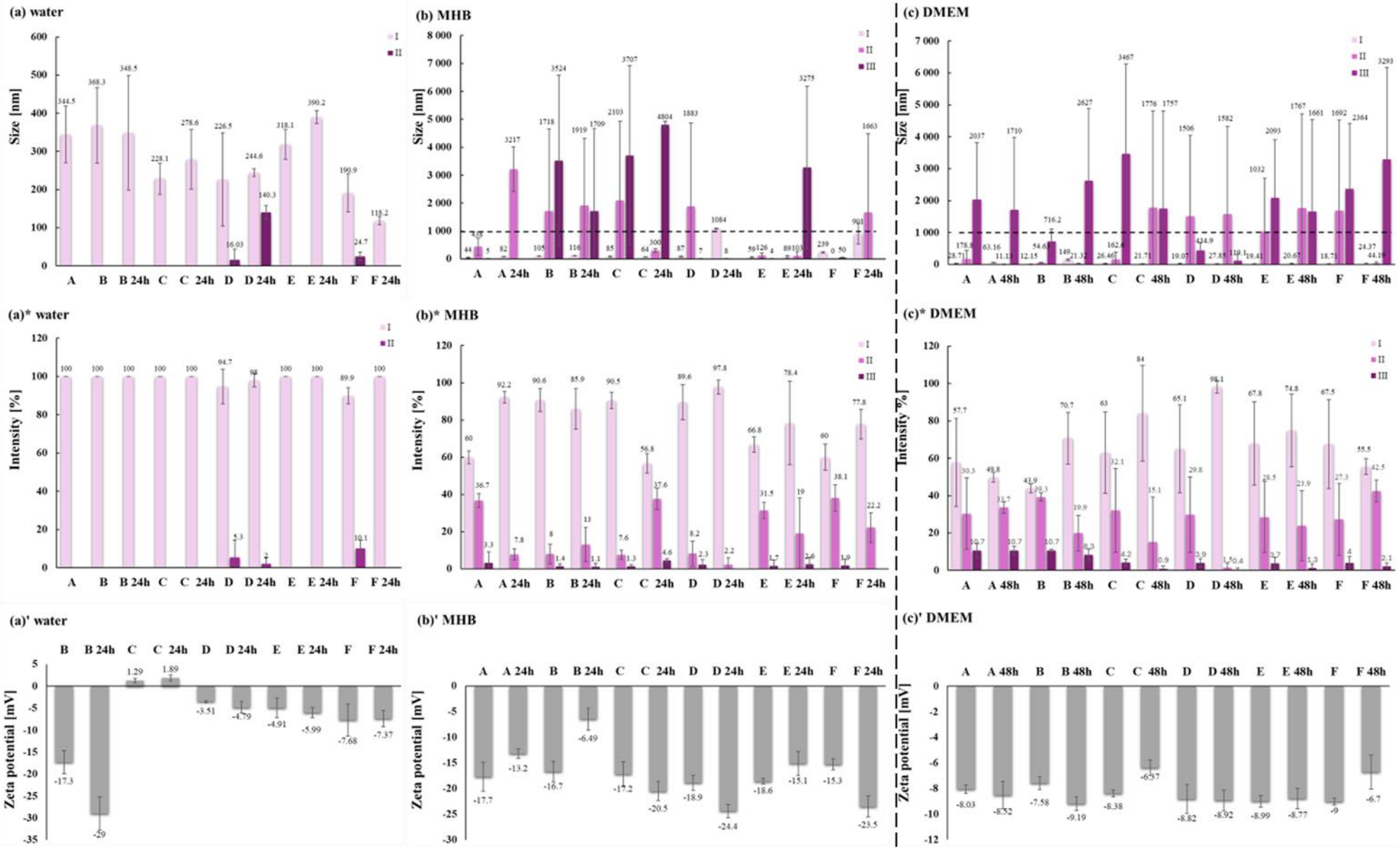

Sample designations in the graphs a, a* and a'

A	distilled water
B	water + DMSO 5%
B 24h	water + DMSO 5% after 24h incubation
C	water + [Ru^{III}(3-HPA)]; 0.5 mg/mL
C 24h	water + [Ru^{III}(3-HPA)]; 0.5 mg/mL; after 24h incubation
D	water + [Ru^{III}(3-HPA)]; 0.0312 mg/mL
D 24h	water + [Ru^{III}(3-HPA)];0.0312 mg/mL; after 24h incubation
E	water + [Ru^{III}(Nic)]; 0.5 mg/mL
E 24h	water + [Ru^{III}(Nic)]; 0.5 mg/mL; after 48h incubation
F	water + [Ru^{III}(Nic)]; 0.0312 mg/mL
F 24h	water + [Ru^{III}(Nic)]; 0.0312 mg/mL; after 48h incubation

Sample designations in the graphs b, b* and b'

A	MHB medium
A 24h	MHB medium after 24h incubation
B	MHB + DMSO 5%
B 24h	MHB + DMSO 5% after 24h incubation
C	MHB + [Ru^{III}(3-HPA)]; 0.5 mg/mL
C 24h	MHB + [Ru^{III}(3-HPA)]; 0.5 mg/mL; after 24h incubation
D	MHB + [Ru^{III}(3-HPA)]; 0.0312 mg/mL
D 24h	MHB + [Ru^{III}(3-HPA)];0.0312 mg/mL; after 24h incubation
E	MHB + [Ru^{III}(Nic)]; 0.5 mg/mL
E 24h	MHB + [Ru^{III}(Nic)]; 0.5 mg/mL; after 48h incubation
F	DMEM + [Ru^{III}(Nic)]; 0.0312 mg/mL
F 24h	MHB + [Ru^{III}(Nic)]; 0.0312 mg/mL; after 48h incubation

Sample designations in the graphs c, c* and c'

A	DMEM medium
A 48h	DMEM medium after 48h incubation
B	DMEM + DMSO 0.5%
B 48h	DMEM + DMSO 0.5% after 48h incubation
C	DMEM + [Ru^{III}(3-HPA)]; 0.5 mg/mL
C 48h	DMEM + [Ru^{III}(3-HPA)]; 0.5 mg/mL; after 48h incubation
D	DMEM + [Ru^{III}(3-HPA)]; 0.025 mg/mL
D 48h	DMEM + [Ru^{III}(3-HPA)];0.025 mg/mL; after 48h incubation
E	DMEM + [Ru^{III}(Nic)]; 0.5 mg/mL
E 48h	DMEM + [Ru^{III}(Nic)]; 0.5 mg/mL; after 48h incubation
F	DMEM + [Ru^{III}(Nic)]; 0.025 mg/mL
F 48h	DMEM + [Ru^{III}(Nic)]; 0.025 mg/mL; after 48h incubation

Figure S8. Hydrodynamic size distribution (a–c), intensity (a*–c*), and zeta potential (a'–c') of the recorded populations (I, II, III) in different media: water (a, a*, a'), Mueller-Hinton Broth (MHB) medium (b, b*, b'), and Dulbecco's Modified Eagle Medium (DMEM) (c, c*, c'). Sample designations are indicated below each graph. The tested compounds were analyzed before and after 24 or 48 hours of incubation at 37 °C. In the plot, $[Ru^{III}(3\text{-HPA})]$ represents the complex $[Ru^{III}Cl_2(3\text{-HPA})_2]^-[3\text{-}HH_2PA]^+(EtOH)_2$, while $[Ru^{III}(Nic)]$ corresponds to $[Ru^{III}Cl_4(NIC)_2]^-[(CH_3)_2NH_2]^+DMF$.

Details on solving of the McGarvey equations for the g tensor

For clarity, we approximate the coordination tetrahedra of the $[Ru^{III}Cl_4(Nic)_2]^-$ and $[Ru^{III}Cl_2(3\text{-}HPA)_2]^-$ anions as possessing C_2 symmetry. In this approximation, the principal *z*-axis of the *g* matrix is oriented perpendicular to the RuCl□ and RuCl□O□ planes in [Ru^{III}Cl□(Nic)□]□ and [Ru^{III}Cl□(3-HPA)□]□,respectively, and is approximately aligned with the N−Ru−N direction. The *x* and *y* axes lie within the RuCl□ and RuCl□O□ planes in a way that they pass between Ru−X bonds. This axis orientation was further confirmed by DFT calculations of the *g* tensor:

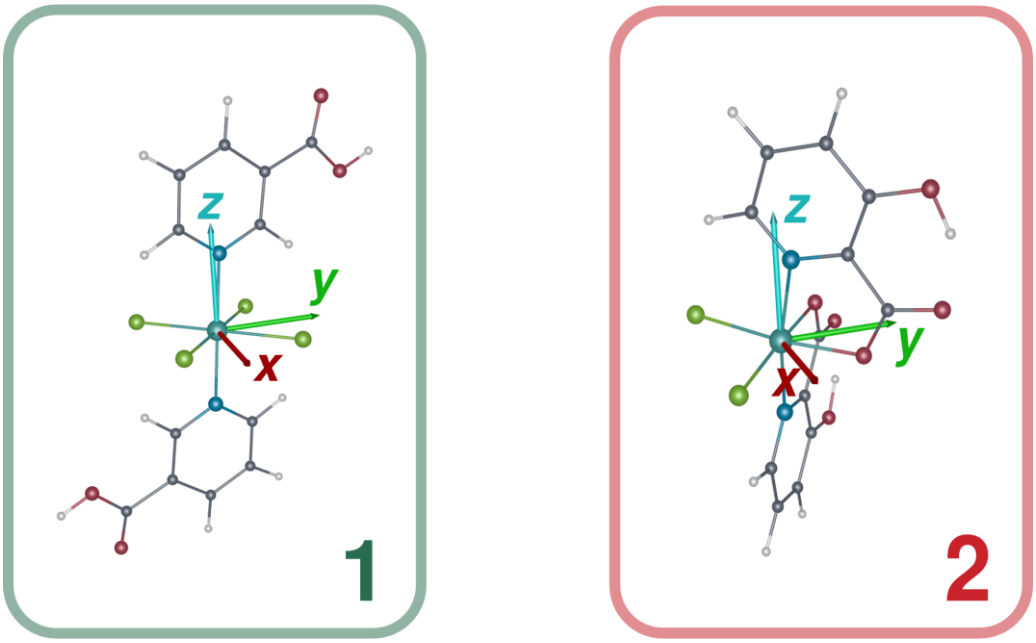

*Orientation of the principal g tensor components within the molecular frame for **1** and **2** as calculated at the BHandLYP level.*

For low-spin d^5 systems, the combined effects of a low-symmetry ligand field and spin-orbit coupling split the T_{2g} level into three well-separated Kramers doublets. The Kramers doublet wavefunctions for the ground state of complexes with C□ symmetry are expressed as:

$$\psi_+ = A\left|xy, \frac{1}{2}\right\rangle + B\left|xz, -\frac{1}{2}\right\rangle + C|yz, -\frac{1}{2}\rangle$$

$$\psi_- = -A\left|xy, -\frac{1}{2}\right\rangle + B\left|xz, \frac{1}{2}\right\rangle - C|yz, \frac{1}{2}\rangle$$

The principal g values are then given by:

$$g_x = 2[B^2 - A^2 - C^2 - 2kAC]$$

$$g_y = 2[C^2 - B^2 - A^2 - 2kAB]$$

$$g_z = 2[A^2 - C^2 - B^2 - 2kBC]$$

where *k* is the orbital reduction factor. The normalization coefficients *A*, *B* and *C* can be used to derive the molecular orbital coefficients *a*, *b* and *c* as follows:

$$A = b;\ B = \frac{(a+c)}{\sqrt{2}};\ C = \frac{(a-c)}{\sqrt{2}}$$

The distortion parameters can then be determined using:

$$\frac{\Delta}{\xi} = \frac{[b(1-b^2)+\sqrt{2}a(1-2a^2)]}{2b(a^2-c^2)}$$

$$\frac{V}{\xi} = \frac{[c(2a+\sqrt{2}b]}{(c^2-a^2)}$$

where Δ and V represent the axial and rhombic ligand field parameters, respectively, and ξ is the one-electron spin-orbit coupling constant. For systems with ideal axial symmetry, c and V are zero.

In the case of these complexes, the value of k is expected to be slightly below 1.0. However, previous studies on pseudo-octahedral systems have reported k values ranging from 0.4 to 1.2 [1], suggesting that the excited states were not well separated from the ground state.

The normalization coefficients A, B and C and the orbital reduction factor k were determined from experimental g factors using particle swarm optimization. Subsequently, the values of a, b, c, Δ/ξ and V/ξ were obtained:

*Solutions of g equations for complex **1** and **2**.*

Complex		g_z	g_y	g_x	A	B	C	k	a	b	c	Δ/ξ	V/ξ
1	**Solution 1**	1.340	-2.558	-2.690	0.934	0.210	0.233	1.063	0.313	0.934	-0.0163	2.60	0.32
	Solution 2	-1.338	-2.561	-2.693	0.698	0.511	0.529	1.138	0.735	0.698	-0.0127	0.36	0.06
	Exp.	1.34	2.56	2.69									
2	**Solution 1**	1.672	-2.450	-2.570	0.973	0.157	0.181	0.937	0.239	0.973	-0.017	3.18	0.55
	Solution 2	1.671	-2.449	-2.570	1.071	0.353	0.387	0.136	0.523	1.071	-0.024	0.30	0.23
	Exp.	1.67	2.45	2.57									

For each complex, two solutions were found that produced g components closely matching the experimental values. However, these solutions differed significantly in the values of Δ/ξ and V/ξ. The solutions labelled as "Solution 2" in the table above should not be considered physically meaningful due to structural aspects: the Δ/ξ value – reflecting axial distortion – is substantially smaller than what is typically expected for an axially distorted low-spin d□ complex [1a,2,3]. In contrast, for **1** and **2**, "Solution 1" appears valid and aligns with previous findings for other strong-field, low-spin d^5 ruthenium(III) and iron(III) complexes with approximate C□ symmetry, including previously reported mixed-valence Ru(II)-Ru(III) ion pairs [1a,2].

The axial distortion parameter Δ/ξ is positive for **1** and **2,** and the larger value of b compared to a and c indicates that the d_{xy} orbital lies above d_{xz} and d_{yz}. Consequently, the electronic configuration of Ru(III) in **1** and **2** is $(d_{xz})^2(d_{yz})^2(d_{xy})^1$. The k values, which are very close to 1.0, along with the smaller values of a and c, suggest that for both complexes, the excited states are well separated from the ground state, resulting in negligible mixing of the lowest Kramers doublet with higher-energy states.

Notably, the calculated rhombic distortion parameter for **1** is less than 60% of the corresponding value for **2**. It aligns well with the more substantial rhombic distortion observed for **2** in X-ray diffraction experiments.

[1] **(a)** M. M. T. Khan, D. Srinivas, R. I. Kureshy, N. H. Khan, Synthesis, Characterization, and EPR Studies of Stable Ruthenium(III) Schiff Base Chloro and Carbonyl Complexes, Inorg. Chem., 1990, **29**, 2320.

(b) O. K. Medhi, U. Agarwala, Electron Spin Resonance Studies of Some Ruthenium(III) Complexes, Inorg. Chem., 1980, **19**, 1381. **(c)** V. T. Coombe, G. A. Heath, T. A. Stephenson, D. A.; Tocher, Electrochemical One-Electron Oxidation of $[Ru(NO)Cl_5]^{2-}$: Spectroscopic and Magnetic Evidence for the (t_{2g}^5) Ruthenium (III) Pentachloronitrosyl Complex Monoanion $[Ru(NO)Cl_5]^-$, J. Chem. Soc., Chem. Commun., 1983, 303.

[2] **(a)** O. Impert, A. Kozakiewicz-Piekarz, A. Katafias, M. Witwicki, U. K. Komarnicka, K. Kurpiewska, R. van Eldik, Mixed-valence outer-sphere Ru^{II}/Ru^{III} ion-pair complexes. Synthesis, experimental, and theoretical studies, Polyhedron, 2022, **223**, 115939. **(b)** B. R. McGarvey, Survey of Ligand Field Parameters of Strong Field D5 Complexes Obtained from the g Matrix, Coord. Chem. Rev., 1998, **170**, 75. **(c)** O. Impert, A. Kozakiewicz, G. Wrzeszcz, A. Katafias, A. Bieńko, R. van Eldik, A. Ozarowski, Characterization of a Mixed-Valence Ru(II)/Ru(III) Ion-Pair Complex. Unexpected High-Frequency Electron Paramagnetic Resonance Evidence for Ru(III)–Ru(III) Dimer Coupling, Inorg. Chem., 2020, **59**, 8609. **(d)** W. M. Reiff, R. E. DeSimone, Electronic Ground States of Dicyanobis(Diimine)Iron(III) Compounds, Inorg. Chem., 1973, **12**, 1793.

[3] M. L. Souza, E. E. Castellano, J. Telser, D. W. Franco, Secondary Coordination Sphere Effects in Ruthenium(III) Tetraammine Complexes: Role of the Coordinated Water Molecule. Inorg. Chem., 2015, **54**, 2067.